



A Mineralogical Investigation on Volatilization of Impurity Elements from Cu-Rich Polymetallic Concentrates During Roasting in Inert Atmosphere

PANDE NISHANT PRASAD, IRIS MCELROY, ANDREAS LENNARTSSON,
and CAISA SAMUELSSON

Four different Cu-rich polymetallic concentrates are tested for volatilization of Sb and As during laboratory-scale roasting. The experiments are performed between 200 °C and 700 °C, at intervals of 100 °C and in an inert atmosphere. Sb volatilization is much less (maximum approximately 45 pct) than As volatilization (maximum approximately 95 pct) in these conditions at 700 °C. As volatilization is however limited from the concentrate having As mainly in a tetrahedrite solid solution ((Cu,Ag,Fe,Zn)₁₂(Sb,As)₄S₁₃). Sb and As retained in the roasted calcine are found in the low-melting liquid phase, formed at approximately 500 °C. This melt phase gets enlarged and enriched in Sb with an increase in temperature. However, there is noticeable As volatilization from this melt phase with the temperature approaching 700 °C. Furthermore, there is an early and relatively high Sb volatilization from the concentrate having Sb substantially as gudmundite. Micron-scale elemental redistribution in gudmundite in the 350 °C roasted calcine confirms its transformation at this temperature. Other Sb minerals did not undergo any detectable transformation at this temperature, suggesting that the significant Sb volatilization starting between 300 °C and 400 °C was primarily from gudmundite. This benign attribute of gudmundite featured in this work in the context of roasting should also be relevant from the geometallurgical perspective during concentrate production, where concentrates bearing Sb are considered substandard for further Cu extraction irrespective of the Sb mineralogy.

<https://doi.org/10.1007/s11663-020-02051-z>

© The Author(s) 2021

I. INTRODUCTION

SULFIDE deposits of copper can broadly be classified as simple or complex. The simple Cu deposits generally comprise copper as the main base metal in the form of chalcopyrite, for instance, the Aitik deposit in northern Sweden.^[1] Complex Cu deposits are polymetallic, usually containing additional base metals (Zn, Pb, Ni, Co, *etc.*), precious metals (Ag, Au, Pt, *etc.*) and the Group 15 elements (As, Sb, Bi). Some examples of complex polymetallic deposits in Sweden are Garpenberg,^[2,3] Maurliden^[4] and Rockliden.^[5] Mineral processing of the ore from these complex deposits generates multiple concentrates, each being rich in a particular base or precious metal. However, these individual

metal-rich concentrates are still polymetallic, containing low proportions of the other metals, and therefore still considered complex for further extraction. For instance, the Cu-rich concentrates studied by Prasad *et al.*^[6] were essentially polymetallic, containing approximately 5 to 10 wt pct Zn, 5 to 15 wt pct Pb, Ag > 250 ppm, As > 0.2 wt pct and Sb > 1.3 wt pct.

The elements As and Sb in the complex concentrates are considered noxious and often referred to as ‘impurity elements,’ owing to the general high toxicity of their compounds.^[7,8] Consequently, the processing of ores bearing As and Sb raises serious environmental concerns. Also, the presence of these elements in the ore tends to degrade the properties of the refined final Cu.^[9]

In the current practice, polymetallic Cu-rich concentrates bearing impurity elements are introduced into the pyrometallurgical extraction process by blending in small proportions with concentrates from the simpler deposits. However, the ongoing depletion of simpler Cu deposits necessitates an increase in the proportions of complex concentrates in the blends to enable a sustainable Cu production in the near future.

PANDE NISHANT PRASAD, ANDREAS LENNARTSSON, and CAISA SAMUELSSON are with the Luleå Tekniska Universitet, 97187 Luleå, Sweden. Contact e-mail: pande.nishant.prasad@ltu.se
IRIS MCELROY is with the Boliden Mines Technology, 93681 Boliden, Sweden.

Manuscript submitted June 26, 2020; accepted December 3, 2020.

Article published online January 6, 2021.

To overcome the associated environmental and metallurgical complexities with blends rich in polymetallic concentrates, the impurity elements, As and Sb should be removed prior to the smelting steps.^[10] The upgrading of As- and Sb-bearing complex concentrates for further processing has been investigated through certain hydrometallurgical treatments. The concentrates were subjected to leaching environments such as acidic chloride^[11–16] and alkaline sulfide^[17–20] for selective dissolution of As and Sb. Alternatively, roasting of Cu-concentrates can also partially volatilize the impurity elements As and Sb.^[21–30] Therefore, advancements in the roasting technology can also facilitate the increase in proportions of the complex concentrates in blends processed for pyrometallurgical Cu extraction.

Heretofore, studies on the As and Sb volatilization during roasting have been performed on the pure As and Sb minerals or on the concentrates rich in specific As or Sb minerals such as enargite (Cu_3AsS_4),^[31,32] arsenopyrite (FeAsS),^[33–35] stibnite (Sb_2S_3)^[36–42] and Sb sulfosalts.^[43] There have also been studies reporting improvements in the Sb volatilization when As and Sb co-exist, owing to complexation in the vapor-phase Sb volatilization.^[44–46] However, in a complex polymetallic concentrate, the behavior of As and Sb minerals may change due to interaction with the other minerals. For instance, Prasad *et al.*^[6] presented an investigation on early sintering susceptibility during roasting due to mineralogical interactions among numerous major and minor minerals existing in Cu-rich polymetallic concentrates. It would be important to investigate the effect of these mineralogical interactions in complex concentrates during roasting on the extents of As and Sb volatilization.

There have also been investigations of As and Sb volatilization using complex concentrates as the starting material for laboratory-scale roasting.^[21,24,26–30,46] However, mineralogical transformations during the volatilization progress in roasted calcines are only moderately discussed. A detailed study of such transformations tracking the deportment of As and Sb in the mineral phases with an increase in temperature is missing, which is the focus of this work. This article discusses the extent of As and Sb removal in the laboratory-scale roasting experiments presented in Prasad *et al.*,^[6] where the complex concentrates experienced sintering during roasting in inert atmosphere. These experiments were performed in inert atmosphere to facilitate a fundamental study on the mineral assemblies in low oxidation potential roasting environments, which are considered favorable for the impurity volatilization.^[47]

This article additionally deliberates on the current practice of strict tolerance on the Sb wt pct content in incoming concentrates at the smelter units, irrespective of the Sb mineralogy.^[25] From the geometallurgical perspective, it is difficult to prevent the entry of Sb sulfosalts minerals (containing Cu, Ag or Pb) into the Cu-rich flotation stream owing to the similarity of their flotation behavior with chalcopyrite.^[5,48,49] The other Sb minerals, particularly the Fe-bearing gudmundite (FeSbS) and berthierite (FeSb_2S_4), lack such flotation

attributes and therefore should ideally end up into the tailings.^[49] However, these Fe-bearing Sb minerals often get misplaced into the Cu-Pb concentrate stream because of their complex association/locking with the main Cu and Pb minerals.^[48] From the metallurgical standpoint, gudmundite in particular, being thermally unstable above 280 ± 10 °C,^[50] may undergo Sb volatilization unlike numerous other Sb minerals found in the complex concentrates. Therefore, the presence of gudmundite in the Cu-rich flotation streams may not create Sb-related complexities in the pyrometallurgical flowsheet of Cu extraction. This hypothesis of the feasibility of Sb volatilization from gudmundite during roasting is also tested in the current work. In the mineral processing context, all Sb minerals are at present aimed for the tailing streams, irrespective of their roasting behavior. The possibility of substantial Sb volatilization from the specific minerals during roasting may be relevant information, also at the stage of concentrate production during mineral processing.

II. EXPERIMENTAL DESIGN AND ANALYTICAL TECHNIQUES

A. Materials

The four Cu-rich complex polymetallic concentrate samples used in this study are listed with their chemical compositions in Table I.

These concentrates belong to the Rockliden, Maurliden and Garpenberg deposits of Boliden Mineral AB, Sweden. To clearly identify the particle-size changes during microscopic studies on the calcines obtained after the roasting, a narrow band of 38 to 53 μm size fraction of these concentrates was used for all the characterizations and experiments, except for one experiment (Experiment Group ID 350-10 in Table II) in which the Rockliden S7574 concentrate size fraction below 38 μm was used. This was because only a limited amount of Rockliden S7574 concentrate was available, generated in a laboratory flotation setup,^[48] and the 38 to 53 μm size fraction of this concentrate got consumed in the previous roasting experiments. Usage of the size fraction < 38 μm in this experiment however did not affect the study in any way since this experiment was performed at 350 °C, at which particle size alterations do not take place because of any physicochemical mineralogical interaction.^[6]

The chemical compositions of the initial concentrates and the roasted calcines were provided by ALS Global AB, Luleå. The method included melting with LiBO_2 , digestion in $\text{HNO}_3/\text{HCl}/\text{HF}$ and measurement using ICP-SFMS in accordance with SS EN ISO 17294-2: 2016^[51] and EPA method 200.8: 1994.^[52]

B. Roasting Experiments in the Vertical Tube Furnace

Experiments on laboratory-scale roasting were performed in a vertical tube furnace setup. These experiments were referred to as the isothermal roasting experiments in Prasad *et al.*^[6] In the beginning of each

Table I. Chemical Composition of Cu-Rich Complex Polymetallic Concentrates Belonging to the 38 to 53 μm Size Fraction

Cu Concentrate	Rockliden S7574	Rockliden 8232	Garpenberg	Maurliden
Cu (Wt Pct)	13.8	16.6	19.3	15.4
Zn (Wt Pct)	8.4	4.7	9.5	4.5
Pb (Wt Pct)	5.2	5	15.3	11.3
Fe (Wt Pct)	25.1	21.6	19.8	31.3
Si (Wt Pct)	0.3	3.8	0.8	0.3
Mg (Wt Pct)	0.1	2.0	0.2	0.1
S (Wt Pct)	31.4	22.6	26.1	33.3
Ag (Wt Pct)	0.03	0.026	1.82	0.036
As (Wt Pct)	0.74	0.44	0.23	2.1
Sb (Wt Pct)	1.36	1.72	2.04	3.77

Data from Prasad *et al.*^[6]

Table II. Details of Laboratory-Scale Roasting Experiments in a Vertical Tube Furnace

Experiment ID	Group	Carrier Gas; Flow Rate, l/min	T , $^{\circ}\text{C}$	Holding Time, min	Sample Initial wt, g	Concentrates Tested
200-1		N_2 ; 5	200	70	10	all 4 concentrates (38-53 μm)
300-1		N_2 ; 5	300	70	10	all 4 concentrates (38-53 μm)
400-1		N_2 ; 5	400	70	10	all 4 concentrates (38-53 μm)
500-1		N_2 ; 5	500	70	10	all 4 concentrates (38-53 μm)
600-1		N_2 ; 5	600	70	10	all 4 concentrates (38-53 μm)
700-1		N_2 ; 5	700	70	10	all 4 concentrates (38-53 μm)
350-10		N_2 ; 2	350	600	50	Rockliden S7574 (< 38 μm)

experiment, the concentrate sample was positioned in a cold zone while the furnace was heating up to the experimental temperature. Once, the desired furnace temperature was achieved, the sample was lifted into the hot zone. The gas atmosphere inside the furnace was maintained inert by flowing nitrogen (Chemical Nitrogen 4.6 from AGA-Linde, purity ≥ 99.996 pct, $\text{H}_2\text{O}(\text{g}) \leq 5$ ppm, $\text{O}_2(\text{g}) \leq 5$ ppm) as a carrier gas.

The various types of experiments with differing operating conditions are listed in Table II.

The experimental apparatus is presented schematically in Figure 1. An optional water-cooled condensation plate shown in Figure 1 was introduced only in the Experiment Group IDs 700-1 and 350-10 to facilitate condensation of volatile species from the gas phase. In the Experiment Group ID 350-10, a longer holding time of 10 h and larger sample mass of 50 g were employed to obtain a sufficient amount of condensates for proper characterization. However, investigations related to these condensate phases are not within the scope of this article.

C. SEM/EDS Analysis

Polished and carbon-coated epoxy mounts were prepared for the initial concentrates and the calcined residues obtained from all the experiments. These epoxy mounts were examined in a Zeiss Merlin FEG SEM (scanning electron microscope) using an Oxford Instruments X-Max EDS (energy-dispersive X-ray

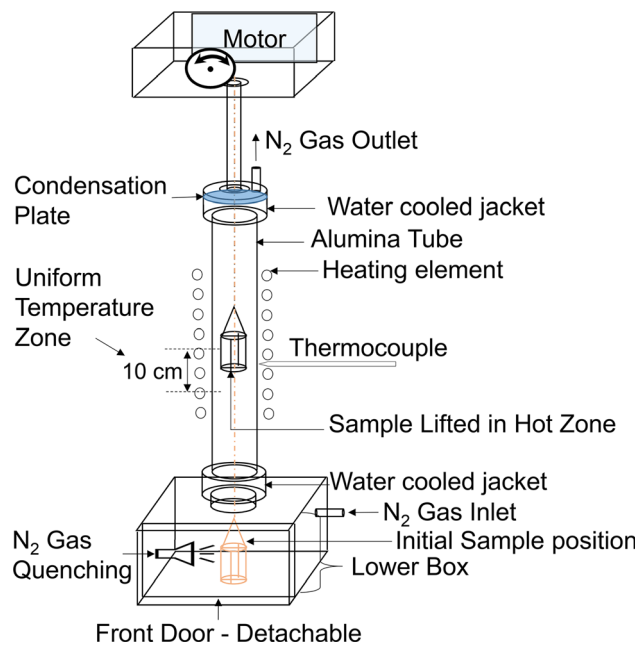


Fig. 1—Vertical tube furnace for roasting of concentrates.

spectroscopy) detector operated by AZtec software. It was operated with a working distance of 8.5 mm, probe current of 1 nA and accelerating voltage of 20 kV. Beam measurement calibration for the EDS analyses was done on pure copper. The EDS spot measurements produced

elemental compositions, which are reported in mol pct after normalization so that the summation of values for all the identified elements is 100 mol pct. Also, EDS-line-scans were performed to detect any microscopic variation in the elemental concentrations in the identified mineral phases.

D. Automated Quantitative Mineralogical Analysis (QEMSCAN)

The epoxy mounts for initial concentrate samples were additionally analyzed in a QEMSCAN system (model: QEMSCAN 650, FEI with W-filament and two Brukar XFlash 5030 EDS detectors) at Boliden Mineral AB, Boliden, Sweden. The programs iMeasure (version 5.4) and iDiscover (version 5.4) were used for data collection and data processing, respectively. The equipment was operated with a working distance of 13 mm, probe current of 10 ± 0.05 nA and accelerating voltage of 25 kV. Measurement was performed in the PMA (particle mineral analysis) mode at a resolution of 2.5 μm , with a field width of 1500 μm (generating 600×600 analysis points per field). Mineral identifications were made using a reference mineral library, SIP (Species Identification Protocol), customized through the numerous in-house mineralogical studies at Boliden AB. This SIP reference library was further modified for adapting

to the mineralogy of the four concentrates using the sampled SEM-EDS measurements of mineral compositions on their epoxy mounts. Table III presents the mineral list with the corresponding elemental composition range set for the SIP definition. Ensuring no compositional overlaps, the elemental ranges were kept wide enough to effectively classify the minerals, especially in the microstructural fields with complex textures.

The QEMSCAN measurements provided mineralogical compositions, liberation and association details by analyzing more than 25,000 particles in each of the four epoxy-mounted concentrate samples (all belonging to the 38 to 53 μm size fraction).

III. RESULTS AND DISCUSSION

A. Sb and As Mineral Department in Initial Concentrates

Figure 2 presents the Sb department in various minerals in the four concentrates obtained from QEMSCAN study.

Evidently, the sulfosalts such as tetrahedrite, bournonite and meneghinite are the major hosts for Sb in the four concentrates. However, Sb also exists significantly in the form of certain non-sulfosalt minerals: (1) gudmundite (approximately 22 wt pct total Sb) in

Table III. Mineral List with the Composition Range Used for the Mineral Library Definition Used in QEMSCAN Measurements

Mineral	Abbreviation	Elemental Range of the Composition Set in SIP										
		Limits, Wt Pct	Cu	Fe	S	Zn	Pb	Ag	Sb	As	Sn	O
Chalcopyrite (CuFeS ₂)	Ccp	Min.	25	23	25	—	—	—	—	—	—	—
		Max.	37	33	40	—	—	—	—	—	—	—
Galena (PbS)	Gn	Min.	0	0	9	0	65	—	—	—	—	—
		Max.	2	2	13	5	90	—	—	—	—	—
Sphalerite ((Zn,Fe)S)	Sph	Min.	0	0.1	20	55	—	—	—	—	—	—
		Max.	3	7	35	65	—	—	—	—	—	—
Pyrite (FeS ₂)	Py	Min.	—	35	40	—	—	—	—	—	—	—
		Max.	—	50	55	—	—	—	—	—	—	—
Tetrahedrite ((Cu,Ag,Fe,Zn) ₁₂ (Sb,As) ₄ S ₁₃) *	Ttr	Min.	25	0.1	20	0.1	—	0.1	15	0	—	—
		Max.	40	8	30	5	—	10	32	5	—	—
Tetrahedrite ((Cu,Ag,Fe,Zn) ₁₂ (Sb,As) ₄ S ₁₃) **	Ttr	Min.	1	0.1	20	0.1	—	0.5	15	0	—	—
		Max.	40	8	30	5	—	40	32	5	—	—
Bournonite (CuPbSbS ₃)	Bour	Min.	10	0	8	—	25	—	15	—	—	—
		Max.	14	1	18	—	40	—	25	—	—	—
Meneghinite (CuPb ₁₃ Sb ₇ S ₂₄)	Mene	Min.	0.1	0	11	—	40	—	12	—	—	—
		Max.	3	2	19	—	70	—	25	—	—	—
Boulangerite (Pb ₅ Sb ₄ S ₁₁)	Boul	Min.	—	—	15	—	50	—	20	—	—	—
		Max.	—	—	25	—	60	—	30	—	—	—
Gudmundite (FeSbS)	Gud	Min.	—	23	12	—	—	—	45	—	—	—
		Max.	—	28	18	—	—	—	60	—	—	—
Silver Antimonides (Ag _n Sb _m) **	Ag-Sb	Min.	0	0	—	—	—	70	20	—	—	—
		Max.	2	2	—	—	—	80	28	—	—	—
Arsenopyrite (FeAsS)	Asy	Min.	—	28	18	—	—	—	—	37	—	—
		Max.	—	37	21	—	—	—	—	44	—	—
Cassiterite (SnO ₂)	Cas	Min.	—	—	—	—	—	—	—	—	75	20
		Max.	—	—	—	—	—	—	—	—	80	25

Data of the elemental range based on sampled EDS measurements on individual concentrate samples. Mineral abbreviations are also listed.

*For all concentrates except Garpenberg.

**Only for Garpenberg concentrate.

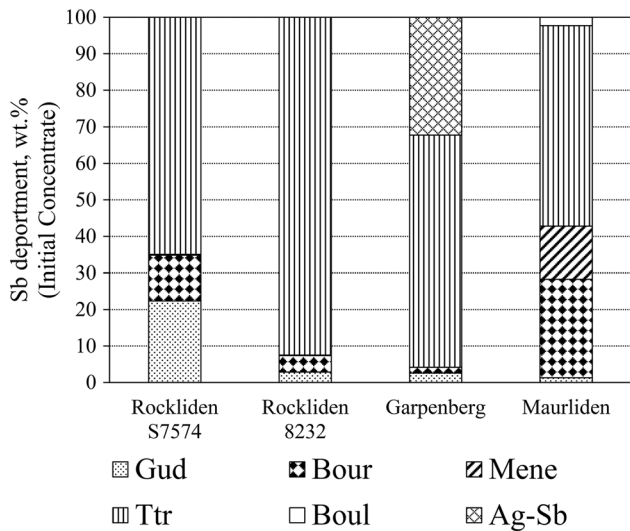


Fig. 2—Sb department in different mineral forms obtained from QEMSCAN analysis of the initial concentrates (38 to 53 μm).

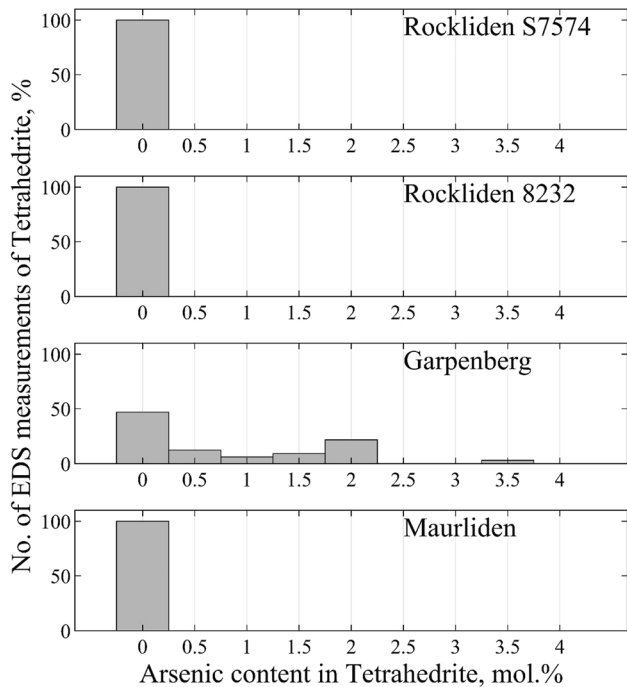


Fig. 3—Histogram showing percentage number of EDS spot measurements on tetrahedrite sites corresponding to different levels of As content (mol pct, x-axis) for the four concentrates.

the Rockliden S7574 concentrate and (2) Ag antimonides (approximately 33 wt pct total Sb, shown as Ag-Sb) in the Garpenberg concentrate.

Regarding the As mineralogy, sampled EDS measurements on the initial concentrates confirmed that arsenopyrite is the main As-bearing mineral in the four concentrates. As is also known to be present in the tetrahedrite solid solution $((\text{Cu,Ag,Fe,Zn})_{12}(\text{Sb,As})_4\text{S}_{13})$ at the sites of Sb in the crystal lattice.^[2] Figure 3 presents histograms showing the percentage number of EDS spot measurements on tetrahedrite in the four

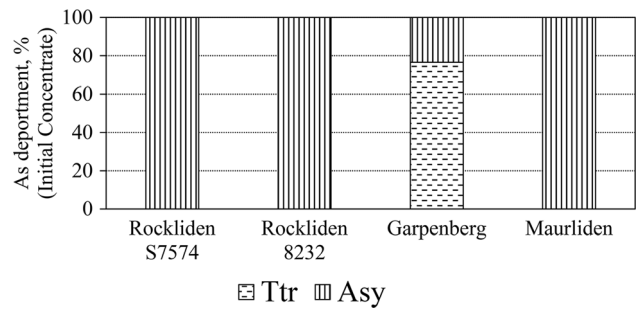


Fig. 4—As department in different mineral forms obtained from QEMSCAN analysis of the initial concentrates (38 to 53 μm), additionally using the chemical composition of Garpenberg concentrate from Table I.

concentrates, belonging to different levels of As content (mol pct, along x-axis). It shows that tetrahedrite hosts As only in the Garpenberg concentrate. As content in the tetrahedrite of the Garpenberg concentrate is up to approximately 3.5 mol pct in the sampled EDS measurements, whereas for the other three concentrates, As is not detected in the tetrahedrite sites.

Due to relatively low accuracy in the composition measurements during QEMSCAN (compared to the spot measurements in SEM-EDS), As-hosting tetrahedrite was not listed as a separate mineral in the SIP (mineral list in Table III). Therefore, the proportion of total As in the Garpenberg concentrate in the form of tetrahedrite was determined by deducting the amount of As in arsenopyrite (wt pct arsenopyrite obtained from QEMSCAN measurement) from the total As content (from the chemical composition of the Garpenberg concentrate in Table I). Accordingly, Figure 4 presents the mineral-wise As department for the four concentrates. It shows that As exists solely as arsenopyrite, except in the Garpenberg concentrate, where a major proportion of As resides in the tetrahedrite solid solution.

B. Sb and As Volatilization During Roasting Experiments

The extents of Sb and As removal from the isothermal roasting experiments performed between 200 $^{\circ}\text{C}$ and 700 $^{\circ}\text{C}$ in intervals of 100 $^{\circ}\text{C}$ (experiment details listed in Table II against the IDs 200-1, 300-1, 400-1, 500-1, 600-1 and 700-1) are shown in Figure 5.

The Sb and As volatilization was calculated using Eq. [1]^[28]:

$$\eta_m = \left[1 - \frac{C_m^f W_f}{C_m^i W_i} \right] \times 100, \quad m = \text{Sb, As} \quad [1]$$

η_m is the extent of element (Sb or As) removal (pct) through volatilization. W_i and W_f are the weights of the initial concentrates and the roasted calcines, respectively ($W_i = 10 \text{ g}$). C_m^i and C_m^f are the wt pct Sb or As content in the initial concentrates and the roasted calcines, respectively (i, initial; f, final, *i.e.*, after roasting; m, As or Sb). The experimental results required for the calculation of η_m are listed in Table IV.

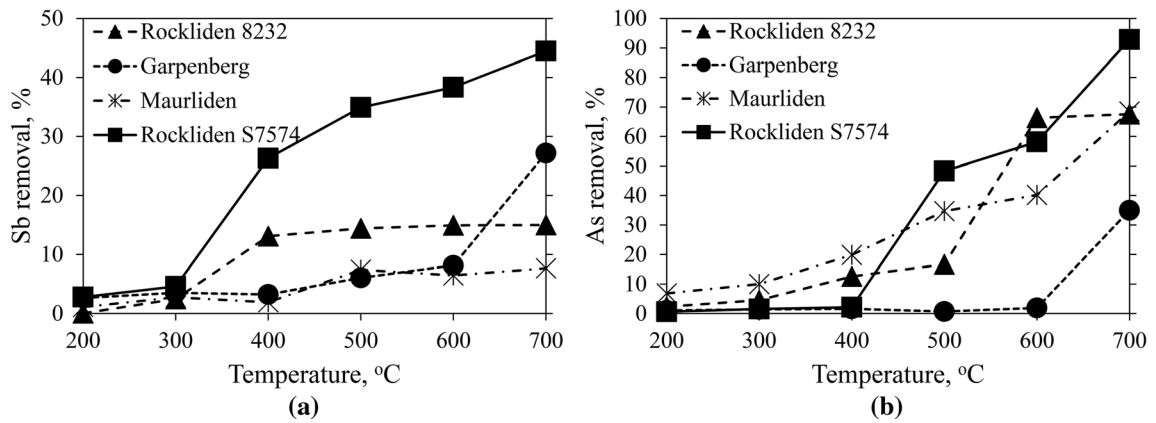


Fig. 5—Extent of impurity removal during the laboratory-scale roasting experiments performed at different temperatures on the four concentrates. (a) Sb removal; (b) As removal.

Among all the concentrates, Sb removal (pct) was the highest from the Rockliden S7574 concentrate (Figure 5(a)). Significant Sb removal from this concentrate was realized from 400 °C onwards. Noticeably, the Rockliden S7574 concentrate had the non-sulfosalt Sb mineral gudmundite (FeSbS) in a relatively high proportion (Figure 2). Investigations on the possibility of gudmundite responsible for the significant Sb volatilization from the Rockliden S7574 concentrate will be presented in a subsequent section.

In Figure 5, As removal is shown to be higher than the Sb removal for most of the concentrates, owing to the low volatility of Sb from the sulfosalt minerals.^[43] Previous experimental^[28,32,53] and model-based theoretical studies^[54] have also corroborated a high As volatilization of > 90 pct in inert atmosphere at 700 °C from concentrates comprising As minerals such as enargite (Cu₃AsS₄)^[32,54] and tennantite (Cu₁₂As₄S₁₃).^[28,53] In the current investigation, As content at 700 °C was highest in the Maurliden concentrate, which also had the highest initial As content (Table IV). However, the extent of As removal (η_{As} , pct) was least from the Garpenberg concentrate (Figure 5b), which remained insignificant up to 600 °C and increased slightly at 700 °C. Notably, the Garpenberg concentrate had a substantial proportion (approximately 78 pct, Figure 4) of As in the tetrahedrite solid solution ((Cu,Ag,Fe,Zn)₁₂(Sb,As)₄S₁₃), unlike in the other three concentrates where As was found solely as arsenopyrite (FeAsS). This suggests that volatilization of As from the tetrahedrite solid solution is lower than from arsenopyrite during roasting of complex concentrates in inert atmosphere up to 700 °C. Similar wide variations (between 19 and 100 pct of As volatilization after 15 min of laboratory-scale roasting at 700 °C in inert atmosphere) were reported by Björkman *et al.*,^[55] consequent to the difference in initial As mineralogy. Also, Chakraborti *et al.*^[33] found that at 525 °C, the As volatilization from arsenopyrite (pure or with small amounts of silica) under inert atmosphere (He) was between 10 and 12 pct. Higher As removal of between 15 and 50 pct at 500 °C found in this work from the

arsenopyrite bearing concentrates (Figure 5(b)) suggests the enhancement of As volatilization in the presence of other minerals co-existing in the complex concentrates.

1. Phases retaining residual As and Sb

An another prominent effect of concentrate mineralogy, *viz.* the sintering tendency in the calcine during roasting, was highlighted by Prasad *et al.*^[6] They reported that certain combinations of minerals such as galena + arsenopyrite + pyrite and galena + tetrahedrite can lead to liquid-phase formation at around 500 °C, causing early sintering. This liquid phase was found to solidify either as a single phase in case of arsenopyrite-bearing concentrates or as an intergrowth of galena and pseudo-tetrahedrite (phase resembling tetrahedrite/skinnerite, hereafter also referred to as PT) for the concentrates low in arsenopyrite. These melt fractions at 500 °C were shown to be particularly rich in As and Sb contents. This article extends those results and in Figure 6 and Table V further presents the micrographs and EDS compositions of the Sb- and As-bearing solidified melt phases from the 600 °C and 700 °C calcines.

In Figure 6, the liquid phases formed in the Rockliden 8232 and Garpenberg concentrates solidified as intergrowths, whereas the intergrown textures are missing in the solidified melts corresponding to the Rockliden S7574 and Maurliden concentrates. This difference in the texture of solidified melts was also evident in the micrographs pertaining to roasting at 500 °C^[6] and was attributed to the relatively high arsenopyrite contents in the Maurliden and Rockliden S7574 concentrates (Maurliden and Rockliden S7574 concentrates are high in As contents, Table I, and arsenopyrite is the only As mineral in these concentrates).

The mineral phases in the fine intergrown texture, M2, appearing in Figure 6 in the micrographs of Rockliden 8232 and Garpenberg concentrates are galena and pseudo-tetrahedrite (PT), established through multiple EDS measurements. Additionally, M3, the texture with a relatively coarser intergrowth, appearing in the

Table IV. Sb and As Content and Final Weight of Calcines Obtained from the Laboratory-Scale Roasting Experiments

Concentrate	Temperature	C_{Sb}^f (Sb, Wt Pct)	C_{As}^f (As, Wt Pct)	W_f (g)
Rockliden S7574	initial	1.36 (C_{Sb}^i)	0.74 (C_{As}^i)	10 (W_i)
	200 °C	1.33	0.74	9.94
	300 °C	1.30	0.73	9.98
	400 °C	1.01	0.73	9.92
	500 °C	0.90	0.39	9.81
	600 °C	0.89	0.33	9.41
	700 °C	0.87	0.06	8.66
Rockliden 8232	initial	1.72 (C_{Sb}^i)	0.44 (C_{As}^i)	10 (W_i)
	200 °C	1.74	0.44	9.88
	300 °C	1.71	0.43	9.81
	400 °C	1.57	0.40	52
	500 °C	1.63	0.40	9.03
	600 °C	1.64	0.17	8.92
	700 °C	1.65	0.16	8.86
Garpenberg	initial	2.04 (C_{Sb}^i)	0.23 (C_{As}^i)	10 (W_i)
	200 °C	1.99	0.23	9.98
	300 °C	1.97	0.23	9.99
	400 °C	1.98	0.23	9.97
	500 °C	1.93	0.23	9.93
	600 °C	1.91	0.23	9.81
	700 °C	1.53	0.15	9.71
Maurliden	initial	3.27 (C_{Sb}^i)	2.10 (C_{As}^i)	10 (W_i)
	200 °C	3.24	1.96	9.98
	300 °C	3.18	1.89	10.00
	400 °C	3.24	1.70	9.90
	500 °C	3.07	1.39	9.86
	600 °C	3.24	1.33	9.44
	700 °C	3.34	0.73	9.04

Garpenberg concentrate at 600 °C, comprises galena and the iss-phase^[56,57] also corroborated in Prasad *et al.*^[6]

The micrographs in Figure 6 also suggest an increased partial melting of galena at 600 °C and 700 °C (marked as PGn in the micrographs), subsequent to the melting initiation at approximately 500 °C.^[6] Partial melting of galena is more profound in the Garpenberg and Maurliden concentrates (since these concentrates are relatively rich in Pb, Table I). The galena from this partial melting (marked as PGn in Figure 6) adjoins the intergrown phase in the micrograph for Garpenberg at 700 °C. PGn also appears as entrapped, rounded, irregular shapes around the other melt phase (M1) in the micrographs for Maurliden at 600 °C and 700 °C. These features in the solidified melt microstructures suggest the co-existence of multiple immiscible liquids^[58] at elevated temperatures. These immiscible liquids are found to amalgamate the unmelted/recrystallized fractions (marked as S in Figure 6) by filling the void spaces in the roasted calcines.

The EDS composition of the spots marked as '⊗' in Figure 6 for the 600 °C and 700 °C calcines are presented in Table V. These spots belong to either PT—the pseudo-tetrahedrite phase in the intergrowths (in M2 for the Rockliden 8232 and Garpenberg concentrates)—or to M1—the solidified single phase (for the Rockliden S7574 and Maurliden concentrates). In the 500 °C calcines,^[6] these phase fractions were found

to be relatively rich in As and Sb contents. Here again, at 600 °C and 700 °C (Table V), the Sb and As contents in PT and M1 are found to be high, suggesting the retention of the unvolatilized Sb and As in these melt phases. Increasing the temperature from 600 °C to 700 °C led to further enrichment of Sb in these liquid phase fractions for all the concentrates. However, the As content was slightly reduced for the Maurliden and Garpenberg concentrates and completely diminished for the Rockliden S7574 and Rockliden 8232 concentrates from 600 °C to 700 °C (Table V). These composition measurements suggest that As was partially volatilized from the melt phase, whereas the Sb was mostly retained.

C. Gudmundite Decomposition in Rockliden S7574 Concentrate During Roasting at 350 °C

To ascertain the likely role of gudmundite in the early and high volatilization of Sb from the Rockliden S7574 concentrate compared to the other concentrates, a roasting experiment was performed at 350 °C (Experiment Type ID 350-10, Table II). This temperature was selected since gudmundite is understood to be unstable above 280 °C.^[50] Second, there was a significant increase in Sb volatilization between 300 °C and 400 °C (Figure 5(a)), and an intermediate temperature (350 °C) could possibly reveal details of the reaction initiation. Third, it would prevent the

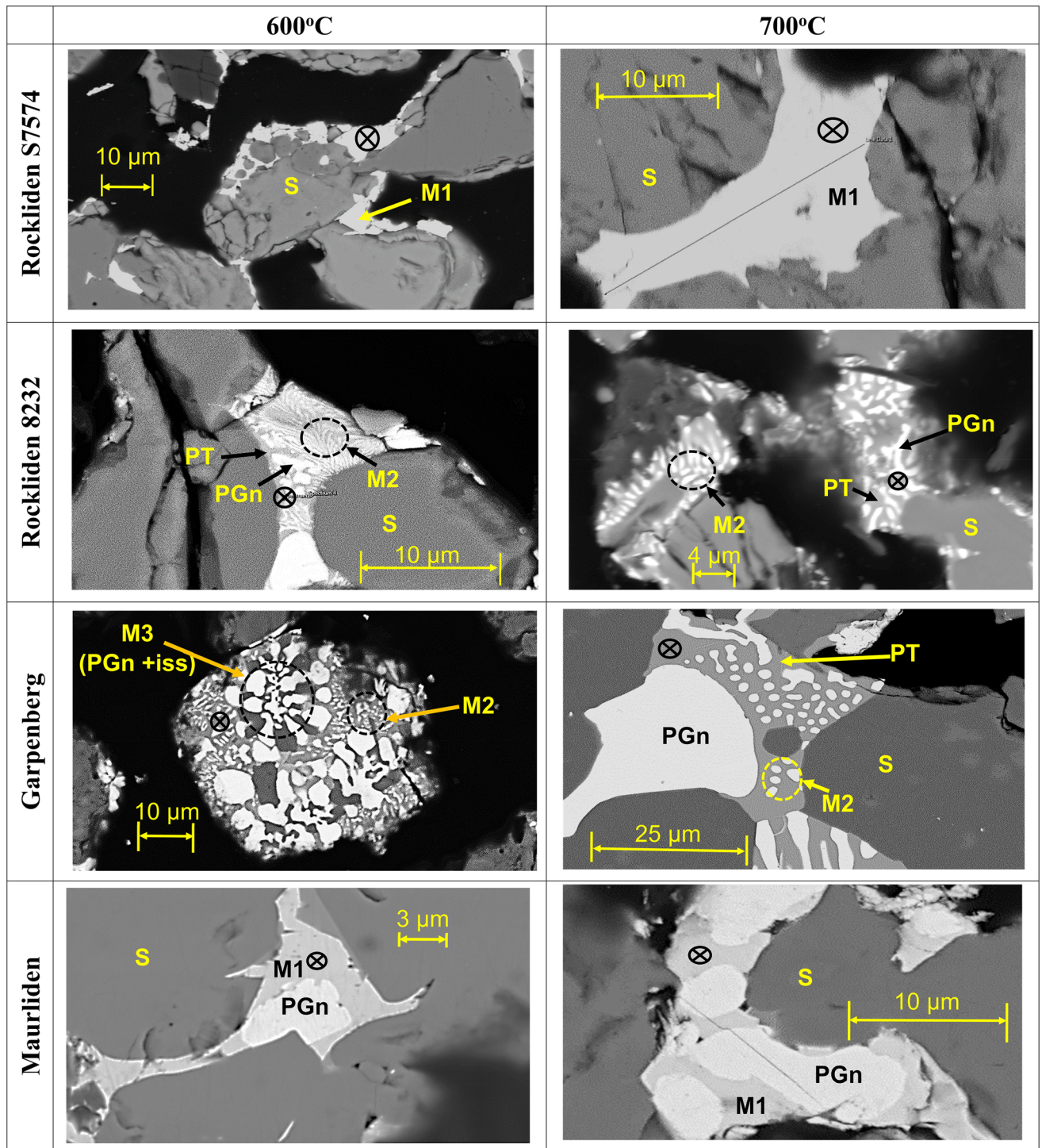


Fig. 6—BSE images showing the melt phases formed during roasting of the concentrates (38 to 53 μm) at 600 °C and 700 °C. M1: melt solidified as a single phase (in concentrates high in arsenopyrite); M2: melt solidified as fine intergrowth of galena (undergoing partial melting) and pseudo-tetrahedrite; M3: melt solidified as coarse intergrowth of galena and iss phase; PGn: galena from partial melting; PT: pseudo-tetrahedrite; S: unmelted/recrystallized phase in the calcine. Location of EDS spot measurements are shown as ‘⊗’ for the melt phase constituents bearing Sb and As.

transformation of other As and Sb minerals (arsenopyrite, sulfosalts and Ag antimonides), which are known to be stable at this temperature.^[59–61] The holding time in this experiment at the reaction

temperature was prolonged from 70 min in the other experiments to 10 h to facilitate a noticeable microstructural evolution due to any mineralogical transformation

Table V. EDS Composition for Measurements at Spots in the Melt Phases Bearing Sb and As Marked as ‘⊗’ in Fig. 6

Concentrate	Temp, °C	S, Mol Pct	Cu, Mol Pct	Fe, Mol Pct	Zn, Mol Pct	Ag, Mol Pct	As, Mol Pct	Sb, Mol Pct	Pb, Mol Pct
Rockliden	600	51.7	1.7	2.9	0	0	3.6	16.7	23.4
S7574	700	50	2.9	3.5	0	0	0	15.2	28.4
Rockliden	600	44.7	28.7	15.2	1.4	0.1	0.3	7.7	2
8232	700	42.8	31.1	6.8	2	0.3	0	12.3	4.7
Garpenberg	600	43	30.3	6.3	0	3.3	2.5	10.8	3.8
	700	24.3	33.5	4.8	3.2	7.5	2.3	24.4	0
Maurliden	600	51.6	2.1	3.4	1.7	0	6	12.8	22.5
	700	52.7	1.1	1.4	0	0	5.4	15.4	24

1. *Gudmundite in the initial concentrate*

To locate the transformed gudmundite in the roasted calcine during microscopy, its nature of occurrence in the initial concentrate was determined, to start with. The QEMSCAN study facilitated this by providing quantified details of the mineral association in the concentrates. Scanning an epoxy sample surface in QEMSCAN generated pixel-wise information (pixel-size depending on scanning resolution), which was used to quantify the complexity in microstructural textures. For this quantification, two minerals were considered associated if a pixel of one of the minerals occurred adjacent to a pixel of the other mineral. The tabulated Figure 7 is a semi-pictorial representation of the ‘Association’ values for all identified minerals in the Rockliden S7574 concentrate. For each mineral, the ‘Association’ values are listed in vertical columns, adding up to 100 pct. Each value represents the percentage number of boundary pixels of the mineral mentioned in the column header (vertical) which touch the pixels of the other mineral mentioned in the corresponding row header (horizontal). For enhanced visualization, the individual cells in Figure 7 are conditionally filled with different gray levels, such that the cell with the highest ‘Association’ value appears darkest, and the cell with the lowest value appears brightest. Cells with ‘Association’ values corresponding to the background (*i.e.*, the portions of the epoxy material on the polished surface) are not included in this conditional cell formatting.

Noticeably, the ‘Association’ value of gudmundite with chalcopyrite is the highest, implying that the gudmundite-chalcopyrite is the most complex binary texture in the Rockliden S7574 concentrate. Figure 8 presents the BSE (back-scattered electron) image and the corresponding false-color image (both from QEMSCAN) of a particle hosting a typical gudmundite-chalcopyrite association found in the Rockliden S7574 concentrate.

The gudmundite-chalcopyrite association is in the form of a complex intergrowth texture, as presented in the BSE image in Figure 8(a). The false-colored image (Figure 8(b)) illustrates the pixel-wise mineral identification done in the QEMSCAN. The false color image is nearly representative of the actual texture of mineral association confirming a reasonable accuracy in mineral

	Ttr	Gn	Sph	Py	Ccp	Asy	Bour	Gud	Cas	Mene	Boul	Sil ³	Otr ⁴	Unc ⁵
Bkd ^{1,2}	58.1	32.6	67.6	69.9	67.6	38.7	42.1	27.7	39.0	6.4	33.5	70.3	48.9	40.8
Ttr	0.0	1.1	1.0	0.3	2.1	0.2	8.7	3.7	0.0	5.5	3.5	0.1	0.1	1.1
Gn	4.6	0.0	4.3	1.8	1.6	2.0	7.6	3.5	0.6	45.1	26.2	0.4	0.5	2.8
Sph	4.6	12.2	0.0	2.5	4.7	2.5	5.9	1.8	2.9	1.4	2.3	0.9	3.8	10.5
Py	4.3	10.7	5.3	0.0	11.5	19.5	5.7	2.8	4.4	2.3	4.6	3.0	4.5	23.2
Ccp	17.4	21.3	9.8	12.1	0.0	14.0	13.1	46.3	8.7	3.5	1.9	7.7	8.9	15.6
Asy	0.1	0.4	0.2	1.0	0.6	0.0	0.5	0.3	0.2	0.4	0.8	0.2	0.6	2.0
Bour	3.6	3.5	0.3	0.1	0.5	0.3	0.0	0.5	0.4	21.5	15.4	0.1	0.1	0.6
Gud	0.9	5.7	0.1	0.1	3.2	0.1	0.4	0.0	0.0	3.5	3.5	0.1	0.6	0.3
Cas	0.0	0.0	0.0	0.0	0.0	0.0	0.0	0.0	0.0	0.0	0.0	0.0	0.0	0.1
Mene	0.1	0.2	0.0	0.0	0.0	0.0	1.0	0.2	0.0	0.0	5.8	0.0	0.1	0.0
Boul	0.0	2.8	0.0	0.0	0.0	0.0	0.4	0.1	0.0	3.1	0.0	0.0	0.0	0.0
Sil ³	0.0	0.1	0.2	0.2	0.5	0.4	0.3	0.7	0.4	0.0	0.4	0.0	0.7	2.6
Otr ⁴	0.0	0.0	0.0	0.0	0.0	0.1	0.0	0.3	0.2	0.4	0.0	0.1	0.0	0.3
Unc ⁵	6.2	9.3	11.2	11.8	7.7	22.3	14.4	12.0	43.2	7.0	2.3	17.2	31.0	0.0
Σ	100.0	100.0	100.0	100.0	100.0	100.0	100.0	100.0	100.0	100.0	100.0	100.0	100.0	100.0

1- Bkd=Background; 3- Sil=Silicates; 4- Otr=Others;

5- Unc=Unclassified

2- The association values with the background are not included in the cell-color formatting

Fig. 7—‘Association’ values obtained from the QEMSCAN study, quantifying the mineral association in Rockliden S7574 concentrate (38 to 53 μm). Two minerals are considered associated if a pixel of one of the minerals occurs adjacent to a pixel of the other mineral. Individual cells are colored/formatted on a gray scale, *i.e.*, the cell with the lowest value appears brightest and the cell with the highest value appears darkest.

identification, which can be attributed to the low scanning resolution of 2.5 μm used in the QEMSCAN study.

2. *Transformation in gudmundite after roasting at 350 °C*

SEM-EDS measurements were performed on the calcine roasted at 350 °C (Experiment Type ID 350-10, Table II) to identify the particles having mineral phases similar to the gudmundite composition, especially in the complex intergrowth texture with chalcopyrite. Figure 9 presents the BSE images of a particle in the initial concentrate and another particle in the roasted calcine (350 °C), both comprising mineral phases in intergrowth textures. Compositions of the intergrown phases in the two images in Figure 9 are presented in Table VI.

Gudmundite in the initial concentrate (Figure 9(a) and Table VI, Spot 2, before roasting) has a composition close to its theoretical stoichiometry: Fe = 33.3 mol pct, Sb = 33.3 mol pct and S = 33.3 mol pct. The matrix mineral of the intergrowth in the initial

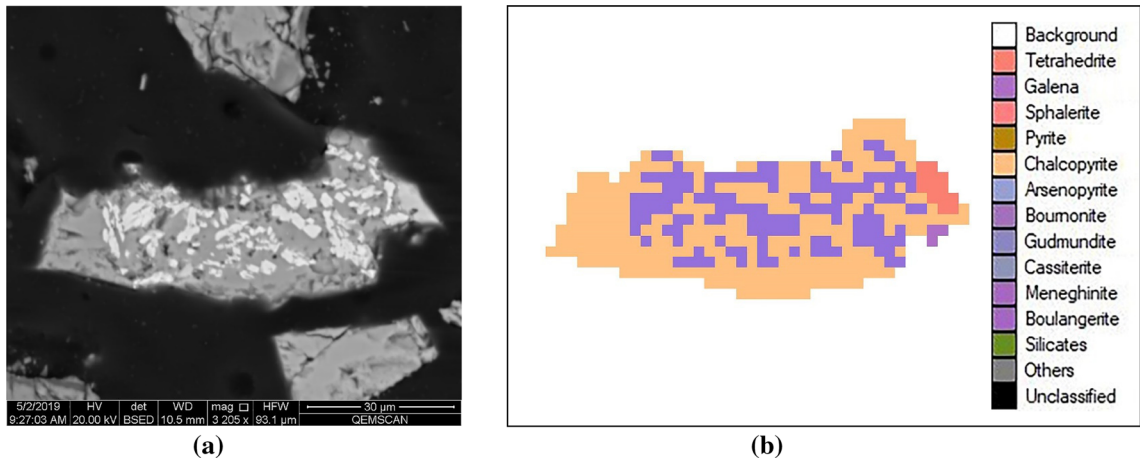


Fig. 8—(a) BSE image of a particle in Rockliden S7574 concentrate (38 to 53 μm size fraction) showing the complex association between gudmundite (bright phase) and chalcocopyrite (grayish phase); (b) falsely colored mineral identification image of the same particle. Both images from QEMSCAN, scanning-resolution/pixel-size being 2.5 μm .

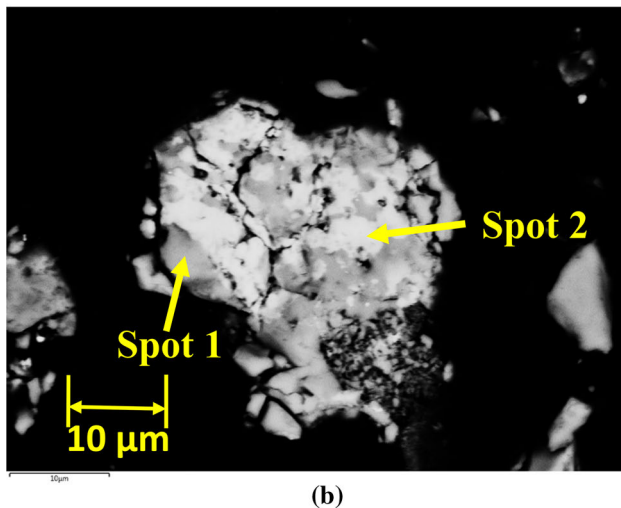
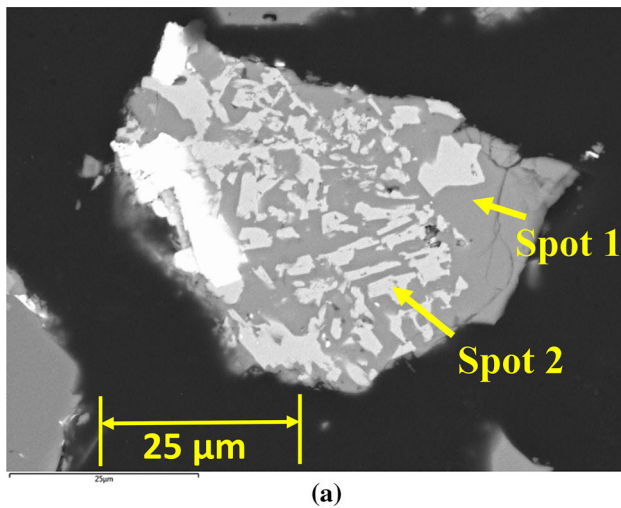


Fig. 9—Particles hosting gudmundite-chalcocopyrite intergrowth belonging to Rockliden S7574 concentrate (a) before roasting; (b) after roasting at 350 $^{\circ}\text{C}$. (a) and (b) Two different particles. Both images obtained from the SEM-EDS measurements. Spots in the regions of single phase with an area $\geq 16 \mu\text{m}^2$ were selected for EDS measurements, located at the tip of the arrows shown in each image.

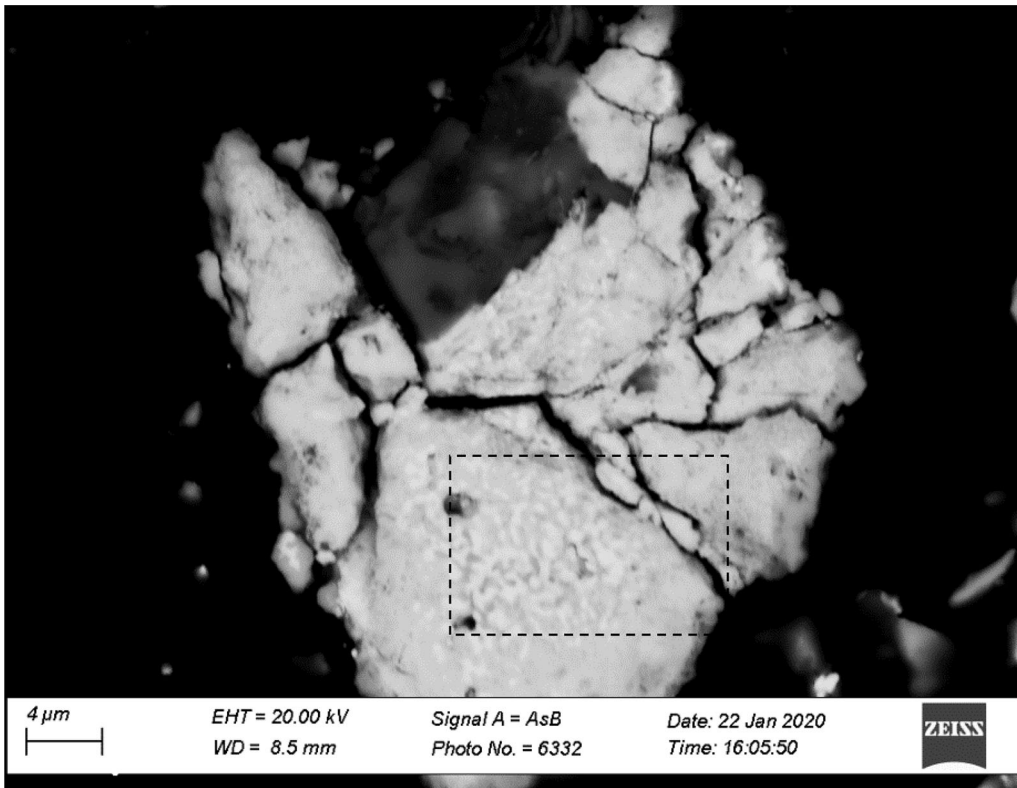
Table VI. Elemental Composition Obtained for the Intergrowth Phases by EDS Measurements at Spots Indicated in Fig. 9(a) for the Initial Concentrate (Rockliden S7574) and in Fig. 9(b) for the Roasted Calcine (350 $^{\circ}\text{C}$)

Element	Rockliden S7574: Chalcocopyrite-Gudmundite Intergrowth			
	Before Roasting		After Roasting at 350 $^{\circ}\text{C}$	
	Spot 1	Spot 2	Spot 1	Spot 2
Cu, Mol Pct	25.6	0.0	16.2	7.8
Fe, Mol Pct	24.8	33.5	30.5	16.8
Zn, Mol Pct	0.0	0.0	2.4	0.6
Sb, Mol Pct	0.0	31.8	0.3	21.6
S, Mol Pct	49.6	34.7	50.7	53.1

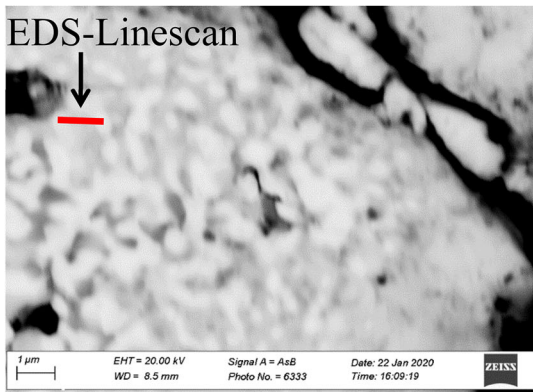
concentrate (Spot 1) is evidently chalcocopyrite (closely matching with the theoretical composition of chalcocopyrite: Cu = 25 mol pct, Fe = 25 mol pct and S = 50 mol pct).

In the roasted calcine, the composition of Spot 1 suggests that the matrix mineral is a partially transformed chalcocopyrite. This partial transformation is likely due to the formation of a solid solution (iss-phase^[56]) during roasting at 350 $^{\circ}\text{C}$ by the assimilation of some amount of sphalerite (noticeable from a 2.4 mol pct Zn content). The composition at Spot 2 in the roasted calcine suggests that the Sb-bearing phase was originally gudmundite (owing to the high values of Fe and Sb contents of 16.8 mol pct and 21.6 mol pct, respectively).

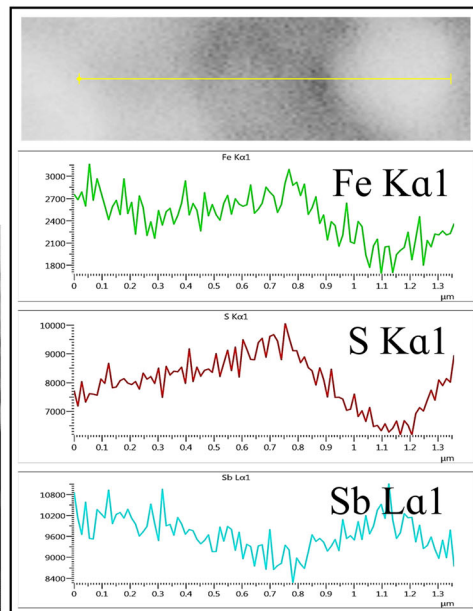
Due to constraints in performing precise EDS measurements over smaller phase areas available in the intergrowths, a sizeable fully liberated particle of original gudmundite was located in the epoxy-mounted sample to study the nature of transformation in gudmundite due to roasting at 350 $^{\circ}\text{C}$. Figures 10(a) through (b) presents the BSE images of this fully



(a)



(b)



(c)

Fig. 10—(a) BSE image of a fully liberated particle of transformed gudmundite in the 350 °C roasted calcine of Rockliden S7574 concentrate, depicting micron-scale elemental redistribution. (b) A magnified view of the rectangular area highlighted in (a), also showing the line segment over which the EDS-linescan was performed. (c) Results of the EDS-linescan (b), presenting the variation in elemental concentration (counts/s) along the line segment.

liberated transformed gudmundite particle (confirmed by numerous EDS spot measurements over this particle). Variation of the gray level over the particle, especially in the highlighted rectangular area (further magnified in Figure 10(b)), suggests a micron-scale

elemental redistribution in gudmundite due to roasting. It was not possible to correctly determine the compositions at the spots with different gray levels due to small size of the uniform phase fields. However, an EDS-linescan was performed to assess the nature of elemental

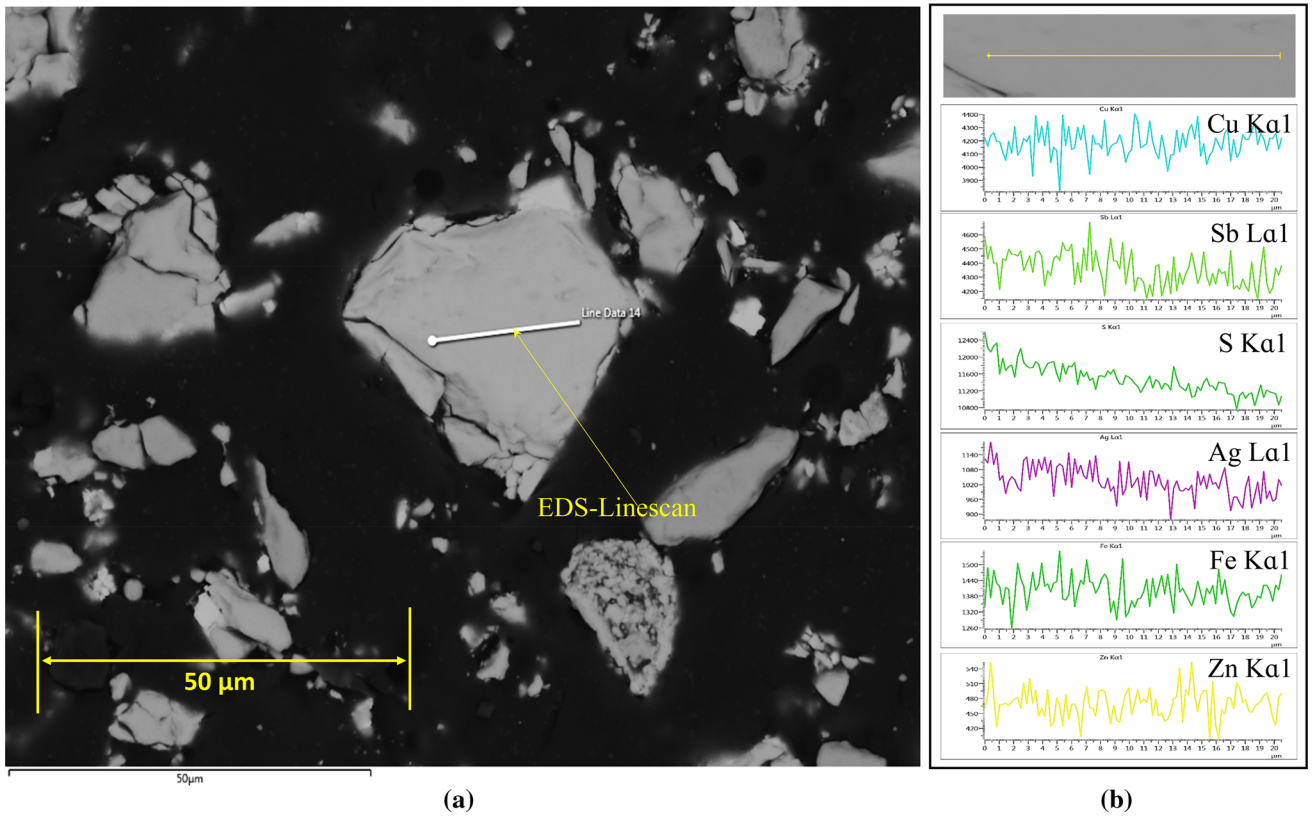


Fig. 11—(a) BSE image and (b) EDS-linescan results for a fully liberated particle of tetrahedrite in the 350 °C roasted calcine of Rockliden S7574 concentrate.

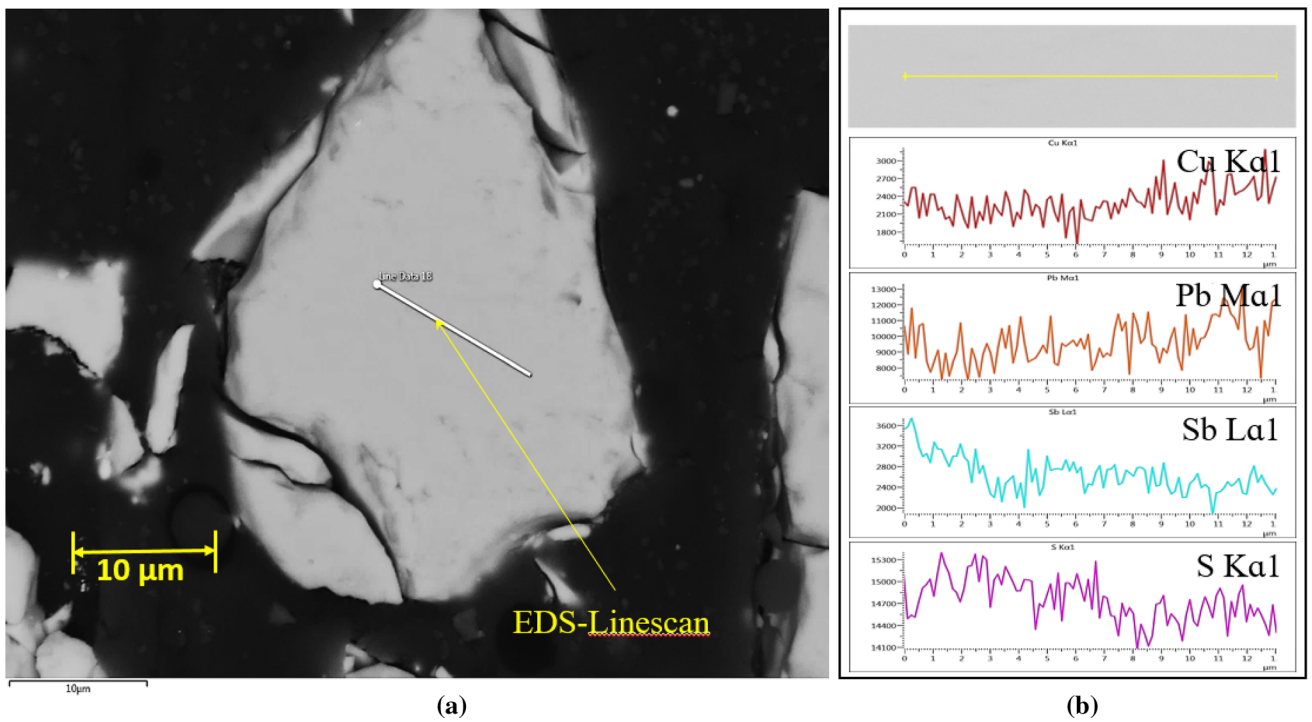
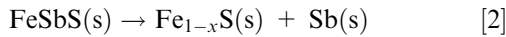


Fig. 12—(a) BSE image and (b) EDS-linescan results for a fully liberated particle of bourmonite in the 350 °C roasted calcine of Rockliden S7574 concentrate.

redistribution, with results presented in Figure 10(c) as plots of element concentration (in counts/s) over the measured line segment. The EDS-linescan shows that the brighter areas in Figure 10(b) are Sb-rich, thereby suggesting the exodus of Sb from the gudmundite (FeSbS). This observation is in agreement with the previous findings of Clark *et al.*^[50] that decomposition of gudmundite takes place *via* Eq. [2] above 280 °C.



D. Transformation in Other Sb Minerals After Roasting at 350 °C

Fully liberated particles of the other Sb-bearing minerals—tetrahedrite and bournonite (Figure 2) in the 350 °C calcine of the Rockliden S7574 concentrate—were also examined in SEM-EDS for the detection of any transformation. BSE images of tetrahedrite (Figure 11) and bournonite (Figure 12(a)) do not show any distinguishable gray-level variation in these mineral particles, suggesting a low probability of transformation in these two minerals. The corresponding EDS-linescan results (Figures 11(b) and 12(b)) further confirm that there is no clear elemental redistribution in tetrahedrite and bournonite at 350 °C, unlike in gudmundite.

Therefore, gudmundite is the only Sb mineral that underwent transformation at 350 °C, decomposing into $\text{Fe}_{1-x}\text{S(s)}$ and Sb(s) . Despite the lack of clarity about the exact reaction mechanism of Sb volatilization subsequently from Sb(s) , findings from the roasting experiment at 350 °C confirm the initial hypothesis proposed in this work. The Rockliden S7574 concentrate being relatively high in gudmundite (Figure 2) and undergoing significant Sb volatilization above 300 °C (Figure 5(a)) suggests that Sb in gudmundite gets effectively volatilized during roasting in inert atmosphere. This benign attribute of gudmundite during roasting may also be relevant in a geometallurgical context, where during flotation in mineral processing the misplacement of gudmundite in a Cu-rich stream is considered troublesome.^[48]

IV. CONCLUSIONS

Prominent findings from the laboratory-scale roasting experiments performed over four different Cu-rich polymetallic concentrates in inert atmosphere are as follows:

- (1) Roasting up to 700 °C in inert atmosphere generally leads to a higher As volatilization compared to Sb volatilization. As volatilization of up to approximately 95 pct could be achieved as against Sb volatilization of a maximum 45 pct in the laboratory-scale experiments. However, if As is primarily in a tetrahedrite solid solution ($(\text{Cu,Ag,Fe,Zn})_{12}(\text{Sb,As})_4\text{S}_{13}$), the As volatilization up to 700 °C from such a concentrate remains insignificant.
- (2) During roasting, Sb and As from the different minerals in the concentrate join a low-melting liquid

phase above 500 °C, formed because of characteristic physicochemical mineral interactions in complex polymetallic concentrates. Increased partial melting of galena with temperature leads to enlargement of the melt phase. This melt phase gets enriched in Sb with an increase in temperature, retaining most of the initial Sb. However, there is noticeable As volatilization from the melt phase with the temperature approaching 700 °C.

- (3) The Sb volatilization from the sulfosalt minerals is insignificant up to 700 °C in inert atmosphere. In contrast, substantial Sb volatilization takes places from gudmundite starting from between 300 °C and 400 °C. Sb volatilization from gudmundite is initiated by its thermal decomposition into $\text{Fe}_{1-x}\text{S(s)}$ and Sb(s) below 400 °C.
- (4) From a geometallurgical perspective, the Sb volatilization characteristics of a Sb mineral such as gudmundite during roasting can be relevant information. For instance, the problem of gudmundite misplacement in the Cu- and Pb-rich flotation streams during mineral processing can be reassessed, considering the beneficial attribute of gudmundite undergoing significant Sb volatilization during roasting in inert atmosphere.

ACKNOWLEDGMENTS

The authors thank (1) CAMM² (Center for Advanced Mining and Metallurgy) at Luleå Tekniska Universitet, Sweden, for the financial support; (2) Swedish Strategic Innovation Program STRIM (a joint venture of Vinnova, Formas and the Swedish Energy Agency) for the financial support; (3) personnel at Boliden AB for providing concentrate samples, chemical analyses and QEMSCAN analyses; (4) Ore Geology at Luleå Tekniska Universitet, Sweden, for providing concentrate samples they produced through laboratory-scale flotation in a previous study.

FUNDING

Open access funding provided by Lulea University of Technology.

OPEN ACCESS

This article is licensed under a Creative Commons Attribution 4.0 International License, which permits use, sharing, adaptation, distribution and reproduction in any medium or format, as long as you give appropriate credit to the original author(s) and the source, provide a link to the Creative Commons licence, and indicate if changes were made. The images or other third party material in this article are included in the article's Creative Commons licence, unless indicated

otherwise in a credit line to the material. If material is not included in the article's Creative Commons licence and your intended use is not permitted by statutory regulation or exceeds the permitted use, you will need to obtain permission directly from the copyright holder. To view a copy of this licence, visit <http://creativecommons.org/licenses/by/4.0/>.

REFERENCES

1. C. Wanhainen, M. Kontturi, and O. Martinsson: *Appl. Earth Sci.*, 2003, vol. 112, pp. 260–67.
2. J. Sandecki and O. Amcoff: *Neues Jahrb. fur Mineral. Abhandlungen*, 1981, vol. 141, pp. 324–40.
3. J. Sandecki: *Neues Jahrb. fur Mineral. Monatshefte*, 1983, pp. 365–74.
4. C. Montelius, R.L. Allen, S.-Å. Svenson, and P. Weihed: *GFF*, 2007, vol. 129, pp. 177–96.
5. F. Minz, N.-J. Bolin, P. Lamberg, and C. Wanhainen: *Miner. Eng.*, 2013, vol. 52, pp. 95–103.
6. P.N. Prasad, A. Lennartsson, and C. Samuelsson: *Metall. Mater. Trans. B*, 2020, vol. 51B, pp. 1446–59.
7. D. Filippou, P. St-Germain, and T. Grammatikopoulos: *Miner. Process. Extr. Metall. Rev.*, 2007, vol. 28, pp. 247–98.
8. P. Grez, R. Schrebler, R. Henriquez, R. Cisternas, M. Orellana, and R. Córdova: *J. Electroanal. Chem.*, 2009, vol. 628, pp. 134–43.
9. S. Wang: *JOM*, 2004, vol. 56, pp. 34–37.
10. C. Samuelsson, and B. Björkman: in *Handbook of Recycling*, E. Worrell and M.A. Reuter, eds., Elsevier, Amsterdam, 2014, pp. 85–94.
11. R. Padilla, D. Girón, and M.C. Ruiz: *Hydrometallurgy*, 2005, vol. 80, pp. 272–79.
12. M.J. Correia, J. Carvalho, and J. Monhemius: *Miner. Eng.*, 2001, vol. 14, pp. 185–95.
13. M.J.N. Correia, J.R. Carvalho, and A.J. Monhemius: *Hydrometallurgy*, 2000, vol. 57, pp. 167–79.
14. S. Guy, C.P. Broadbent, G.J. Lawson, and J.D.J. Jackson: *Hydrometallurgy*, 1983, vol. 10, pp. 243–55.
15. T. Havlik, Z. Ivanova, J. Dvorscikova, and R. Kammel: *Met. (Berlin, West)*, 1999, vol. 53, pp. 390–94.
16. T. Havlik, and R. Kammel: *Met. (Berlin, West)*, 2000, vol. 54, pp. 26–29.
17. P. Baláz and M. Achimovičová: *Hydrometallurgy*, 2006, vol. 84, pp. 60–68.
18. P. Baláz and M. Achimovičová: *Int. J. Miner. Process.*, 2006, vol. 81, pp. 44–50.
19. P. Balaz, R. Kammel, and C. Villachica: *Met. (Berlin, West)*, 2001, vol. 55, pp. 196–200.
20. S.A. Awe, C. Samuelsson, and Å. Sandström: *Hydrometallurgy*, 2010, vol. 103, pp. 167–72.
21. I. Wilkomirsky, F. Parada, A. Ulloa, A. Carrasso, and L. Jeraldo: in *Proc. IV Int. Conf. Clean Technol. Min. Ind.*, vol. 2, Concepción Univ. Press, 1998, pp. 613–21.
22. A. Bjornberg, S.A. Holmstrom, and G. Lindkvist: in *US Pat. 4,626,279*, 1986.
23. M. Devia, I. Wilkomirsky, and R. Parra: *Mining Metall. Explor.*, 2012, vol. 29, pp. 121–28.
24. R. Padilla, and M.C. Ruiz: in *Drying, Roasting, Calcining Miner.*, T. Battle, J. Downey, L. May, B. Davis, N. Neelameggham, S. Sanchez-Segado, and C. Pistorius, eds., Springer, Berlin, 2016, pp. 43–50.
25. P.R. Taylor and T.A.R. Putra: in *Celebrating Megascale*, P.J. Mackey, E.J. Grimsey, R.T. Jones, and G.A. Brooks, eds., Springer, Berlin, 2014, pp. 197–211.
26. W. Hong Lu and Z. Lan Yin: *Int. J. Miner. Process.*, 2016, vol. 153, pp. 1–7.
27. S. Shibuya, C. Tokoro, and T. Okura: in *Proc. 7th Eur. Metall. Conf.*, 2013, pp. 111–22.
28. K. Haga, B. Altansukh, and A. Shibayama: *Mater. Trans.*, 2018, vol. 59, pp. 1396–1403.
29. Å. Holmström: Ph.D. Thesis, R. Inst. Technol., Dep. Prod. Technol. (Stockholm), 1988.
30. I. Wilkomirsky, R. Parra, F. Parada, and E. Balladares: in *COM 2014 - Conf. Metall. Proc.*, B. Davis, ed., Metall. Mater. Soc., Can. Inst. Min. Metall. Pet., 2014.
31. R. Padilla, A. Aracena, and M.C. Ruiz: *Metall. Mater. Trans. B*, 2012, vol. 43B, pp. 1119–26.
32. R. Padilla, Y. Fan, and I. Wilkomirsky: *Can. Metall. Q.*, 2001, vol. 40, pp. 335–42.
33. N. Chakraborti and D.C. Lynch: *Metall. Trans. B*, 1983, vol. 14, pp. 239–51.
34. A. Vian, C. Iriate, and A. Romero: *Ind. Eng. Chem. Process Des. Dev.*, 1963, vol. 2, pp. 214–23.
35. G. Ruihua: *Yunnan Chem. Technol.*, 1995, vol. 3.
36. Y. Yang and Y.X. Hua: *TransMet. Soc. China Engl. Ed.*, 2003, vol. 13, pp. 221–25.
37. W. Qin, H. Luo, W. Liu, Y. Zheng, K. Yang, and J. Han: *J. Cent. South Univ.*, 2015, vol. 22, pp. 868–73.
38. F. Zhu, Y. Hua, and Y. Meng: *Miner. Process. Extr. Metall.*, 2005, vol. 114, pp. 219–23.
39. R. Padilla, G. Ramirez, and M.C. Ruiz: *Metall. Mater. Trans. B*, 2010, vol. 41, pp. 1284–92.
40. Ž. Živković, N. Štrbac, D. Živković, D. Grujičić, and B. Boyanov: *Thermochim. Acta*, 2002, vol. 383, pp. 137–43.
41. R. Padilla, A. Aracena, and M.C. Ruiz: *J. Min. Metall. B Metall.*, 2014, vol. 50, pp. 127–32.
42. Y.X. Hua, Y. Yang, and F.L. Zhu: *J. Mater. Sci. Technol.*, 2003, vol. 19, pp. 619–22.
43. L. Komorova, A. Holmstrom, and I. Imris: *Scand. J. Metall.*, 1985, vol. 14, pp. 103–12.
44. T. Li, and J.P. Hager: in *Reinhardt Schuhmann Int. Symp. Innovative Technol. React. Des. Extr. Metall., Proc. Symp.*, D.R. Gaskell, J.P. Hager, J.E. Hoffmann, and P.J. Mackey, eds., 1986, pp. 845–68.
45. J.E. Mauser: *Metall. Trans. B*, 1982, vol. 13, pp. 511–13.
46. G. Lindkvist and A. Holmstrom: *Adv. Sulfide Smelt.*, 1983, vol. 2, pp. 451–72.
47. S. Nakazawa, A. Yazawa, and F.R.A. Jorgensen: *Metall. Mater. Trans. A Phys. Metall. Mater. Sci.*, 1999, vol. 30, pp. 393–401.
48. F.E. Minz, N.-J. Bolin, P. Lamberg, K. Bachmann, J. Gutzmer, and C. Wanhainen: *Miner. Eng.*, 2015, vol. 82, pp. 125–35.
49. T. Lager and E. Forssberg: *Trans. Inst. Min. Metall. Sect. C-Mineral Process. Extr. Metall.*, 1990, vol. 99, pp. 54–61.
50. A.H. Clark: *Mineral. Mag. J. Mineral. Soc.*, 1966, vol. 36, pp. 1123–25.
51. SS EN ISO 17294-2, Swed. Stand., Eur. Comm. Stand., 2016.
52. S.E. Long and T.D. Martin: *EPA Method 200.8*, U.S. Environ. Prot. Agency, 1994.
53. Z. Yin, W. Lu, and H. Xiao: *Vacuum*, 2014, vol. 101, pp. 350–53.
54. J. Tapia and I. Wilkomirsky: *Min. Metall. Explor.*, 2001, vol. 18, pp. 154–61.
55. B. Björkman, U. Degerstedt, B. Lindblom, and C. Samuelsson: in *Extr. Process. Treat. Minimization Wastes, Proc. Int. Symp.*, J. Hager, ed., Miner. Met. Mater. Soc., 1994, pp. 825–42.
56. S. Kojima and A. Sugaki: *Econ. Geol.*, 1985, vol. 80, pp. 158–71.
57. S. Kojima and A. Sugaki: *Mineral. J.*, 1984, vol. 12, pp. 15–28.
58. N. Derimov and R. Abbaschian: *Entropy*, 2018, vol. 20, p. 890.
59. A.G. Tomkins, D.R.M. Pattison, and B.R. Frost: *J. Petrol.*, 2007, vol. 48, pp. 511–35.
60. B.R. Frost, J.A. Mavrogenes, and A.G. Tomkins: *Can. Mineral.*, 2002, vol. 40, pp. 1–18.
61. A.G. Tomkins, B.R. Frost, and D.R.M. Pattison: *Can. Mineral.*, 2006, vol. 44, pp. 1045–62.

Publisher's Note Springer Nature remains neutral with regard to jurisdictional claims in published maps and institutional affiliations.